IMAGING AND ANALYSIS OF ANGIOGENESIS FOR SKIN TRANSPLANTATION BY MICROANGIOGRAPHY

A.P. Condurache, T. Aach[*]

University of Luebeck
Institute for Signal Processing
Ratzeburger Allee 160,
D-23538 Luebeck, Germany

S. Grzybowski, H.G. Machens

University Hospital of SH
Clinic for Plastic Surgery, Burn Center
Ratzeburger Allee 160,
D-23538 Luebeck, Germany

ABSTRACT

The success of skin transplantations depends on a proper revascularization of the transplanted tissue. Angiogenesis (vessel growth) in the transplanted dermal matrices can be stimulated by administering different drugs. To evaluate the effectiveness of different drug treatments in an experimental setting using laboratory animals, vessels in transplant samples are visualized by so-called micro-angiograms, i.e., X-ray images after contrast agent injection. We describe a framework for the acquisition of such micro-angiograms as well as for the subsequent semi-automatic analysis of angiogenesis. Central to our analysis is the segmentation of small fasciocutaneous vessels in the transplant sample.

1. INTRODUCTION

The success of skin transplantation operations depends crucially on the adequate revascularisation of the transplanted dermal matrix. To induce vessel growth or angiogenesis, pharmacological substances may be seeded into the dermal matrix [8]. The purpose of the system described in this paper is to evaluate the effectiveness of different such substances. To this end, dermal matrices were transplanted to cover two disk-shaped full-thickness skin defects (diameter: 15mm) on the backs of laboratory animals (nude mice, body weight about 30g) [9].

1.1. Vessel imaging by micro-angiography

For vessel imaging after a given time interval (3 to 14 days), blood is withdrawn via the left carotid artery using micro-surgical instruments, and slowly replaced by a contrast medium. The transplant sample is then harvested. The collected transplant sample is imaged using an X-ray mammography system (typical settings: 9mAs at 24kV). A micro-angiogram thus obtained shows the fasciocutaneous vessels, potentially down to a size of about $20\mu m$ [9], and is depicted in Fig. 1a.

1.2. Micro-angiography analysis

Once the micro-angiograms are acquired, we seek to quantify the angiogenesis in the target tissue, e.g. by measures such as the percentage of area covered by the blood vessels in the target sample, the vessel length, or the microvascular index (see [9] and the references in there). To this end, the vessels need to be identified in the imaged transplant. Since our system's field of application is an experimental laboratory setting for drug evaluation rather than clinical routine, time-constraints are of less concern, and also a certain degree of interaction is feasible. Apart from the imaging setup described above, the central part of our system is a semiautomatic micro-vessel segmentation algorithm. The results are computed in several iterations starting from an over-segmentation with practically almost no false negatives. The over-segmentation is then thinned out stepwise to produce a result. Since experience shows that these results may contain some false positives and negatives, we store the processing result of each iteration. In a final step the user may then leaf through the different stages of the algorithm, and select the vessel segments.

Our vessel segmentation algorithm first seeks to enhance vessels, before an iterative classification is carried out [11]. Vessel enhancement is based on the following observation [1]: vessels are oriented tubular structures of a certain size with increased absorption relative to their immediate surroundings due to the contrast medium. In [6] tubular structures are enhanced using the eigenvalues of the Hessian matrix computed at different scales. In [13] multiple orientated matched filters are used to enhance directional structures. The multi-scale approach in [1] employs a Laplacian pyramid to analyze vessels in cardiac angiograms according to shape, contrast, and motion while at the same time preventing unacceptable noise boosting.

Vessel segmentation can be done using: region growing

[*]T. Aach is now with Institute of Imaging and Computer Vision, RWTH Aachen University, D-52056 Aachen, Germany.

[14], active contours [15], or tracking [3] as well as by other methods [10]. We also distinguish between fully automatic [3, 10], and semi-automatic [14, 15] vessel segmentation algorithms where the latter typically need some user supplied seed points (points which with a high probability belong to the vessels).

In our micro-angiography problem, we start by enhancing vessel structures by individual methods for larger and mid-sized to small vessels respectively. The results are combined to construct a pixel feature vector space from the analyzed micro-angiogram (Section 2). To segment the vessels we use an iterative unsupervised segmentation algorithm which improves an initial percentile based oversegmentation result. Finally, the user is allowed to access the results from each iteration step, and to select interactively the desired vessels segments. Thus even the small vessels which are hard to separate from the background can be correctly segmented (Section 3). After segmentation, measures such as the absolute or relative vessel area can directly be computed. Since such area-based measures are more influenced by larger vessels than smaller ones, length-based measures such as the micro-vascular index mentioned above can also be calculated after an additional skeletonization procedure such as the one described in [5].

2. MICRO-ANGIOGRAPHY VESSEL FILTERING

The main purpose of the enhancement is to increase separability of the vessel and non-vessel classes. Since in micro-angiograms the variability of the vessels, especially with respect to their diameter, is particularly large, we represent the classes by a three dimensional feature vector, which allows to capture small, mid-sized and large vessel structures. Another objective is to equalize the background, thus representing it by a narrower distribution.

2.1. Background equalization

Since the vessels absorb stronger than their immediate neighborhoods, background may be equalized by a morphological tophat-like operator [5]. This operator is defined as the difference between the original image and its closing. If the filter window size is chosen slightly larger than the largest vessel diameter, the (dark) vessels will be suppressed after image closing, leaving only the background. Subtracting this result from the original yields then predominantly vessel information. The effect of this morphological operator on the separability is twofold. First, it successfully increases the homogeneity of the background pixels. At the same time, assuming an additive image model (which may be obtained by logarithmation) it reduces also the variance of the vessel pixels as their intensities depend not only on the own absorption but also on the absorption of their surrounding background to which they are superimposed. A result is shown in Fig. 1b.

2.2. Homomorphic filter

In angiography, the attenuation of the contrast-agent filled vessels adds to the attenuation of the background. Due to the exponential absorption of X radiation, this addition is turned into a multiplicative relationship between the background tissue image and the contrasted vessel image. The homomorphic filter for multiplicatively combined signals [12] appears therefore suited for vessel enhancement. After initial logarithmation, the two sub-images are additively combined. To eliminate the background and enhance the vessels we apply then a linear, shift-invariant high-pass filter specifically designed to increase the vessel structures. The high frequency components are obtained after subtracting from the original sum its low-pass filtration result. To increase the vessel contrast an amplification of the high-pass channel by a factor larger than one follows. Finally, the exponential of the high-pass filtration result is computed. A result is shown in Fig. 1c. By attenuating the background further, the homomorphic filter can improve the homogeneity of the background and increase the contrast between vessels and background. It is however not especially designed to improve the homogeneity of the vessel class.

2.3. Hessian-based micro-vessel enhancement

To improve the homogeneity of the vessel class, we address the problem of the small to mid-size vessels by means of the eigenvalues of the Hessian matrix [6]. Since vessels are dark tubular structures of limited diameter, we use for enhancement the largest eigenvalue of the Hessian matrix, which takes prominent values only over such structures, within an appropriate range of scale. The size of the structures to which the eigenvalue is sensitive depends on the size of the derivative kernels used as well as on the scale at which the image is analyzed. We seek to capture only the small to mid-sized vessels, since the large vessels do already exhibit sufficient contrast. The vessel map is obtained by seeking the largest Hessian eigenvalue over different scales and combining the results by the maximum rule. By targeting only smaller vessels, the variability between vessels of different sizes is reduced, as is evident from the result in Fig. 1d.

3. VESSEL CLASSIFICATION

We segment the vessels by a fuzzy clustering algorithm which yields better results in comparison to other similar methods [2]. It iteratively improves a clustering performance measure computed on a fuzzy set decomposition, starting from an initial partition (Section 3.1). The algorithm may iterate either until no pixel changes its class

anymore or until a certain number of iterations is reached. After the iteration stops, the user may optionally browse through the results obtained at the end of each iteration, and choose the desired vessel segments (Section 3.2) as described above.

Before classification each component of the pixel feature vector is normalized to the interval $[0, 1]$ to avoid undesired bias toward a certain feature component.

3.1. Fuzzy clustering

The unsupervised classification algorithm [2] separates a feature space by iteratively improving a measure of the partition's quality starting from an initial partition. The initial partition is in our case an over-segmentation result computed by thresholding the vessel map obtained after applying the morphological filter described in Section 2.1 to the original angiogram. Empirically, the vessel covered area is always less than 50% of the image area, thus we choose the 50th percentile as threshold. We ensure thus that in the initial segmentation, practically all vessels are present.

The fuzzy class membership coefficients are computed, using a function which measures how closely related the investigated vector is to a certain class. This function is called affinity. The affinity of a feature vector $\vec{x}$ out of a feature space $U = \{\vec{x}_1, \vec{x}_2, \ldots, \vec{x}_N\}$ with N feature vectors, with respect to ω_i, which is a subset of U obtained from an initial hard partition $\{\omega_1, \omega_2, \ldots, \omega_M\}$ with M classes, is a numerical indicator defined as:

$$r(\vec{x}, \omega_i) = 1 - \frac{1}{N} \sum_{\vec{y} \in \omega_i} h^\beta(\| \vec{x} - \vec{y} \|) \qquad (1)$$

with $h^\beta : [0, \infty) \rightarrow [0, 1]$ and:

$$h^\beta(\nu) = \begin{cases} \frac{\nu^2}{\beta} & \text{if } \nu \leq \sqrt{\beta} \\ 1 & \text{if } \nu > \sqrt{\beta} \end{cases} \qquad (2)$$

Using the affinity function, the class belonging coefficient for vector $\vec{x}$ and class ω_i is defined as: $u_i(\vec{x}) = p_i \frac{r(\vec{x}, \omega_i)}{r(\vec{x}, U)}$, with p_i the prior on ω_i.

The parameter β actually defines a certain region in the feature space within which the feature vectors are allowed to contribute to the affinity computation. In our experiments β was chosen such that $max \parallel \vec{x} - \vec{y} \parallel = \sqrt{\beta}$ for $\vec{x}, \vec{y} \in U$ so that all feature space vectors are used to compute the affinity.

Alternatively if each class ω_i is simply represented by its mean vector alone, the fuzzy class membership coefficients are:

$$u_i(\vec{x}) = \frac{\beta - \parallel \vec{x} - \mu_i \parallel^2}{\beta M - \sum_{j=1}^{M} \parallel \vec{x} - \mu_j \parallel^2} \qquad (3)$$

and $\sum_i^M u_i(\vec{x}) = 1$.

To measure the quality of a certain fuzzy partition (i.e. the amount of incertitude (fuzziness) present), the following function is used:

$$\Psi = \frac{1}{N(M-1)} \sum_{i=1}^{M-1} \sum_{j=i+1}^{M} \sum_{\vec{x} \in U} (u_i(\vec{x}) - u_j(\vec{x}))^2 \qquad (4)$$

with $\Psi \in [0, 1]$ and $\Psi = 0$ indicating the highest possible degree of fuzziness. Using this measure, the algorithm converges properly to an optimal partition only for highly separable feature spaces. If this is not exactly the case (e.g. for vessel segmentation), an additional stopping criterion is needed [4]. In our experiments the algorithm was allowed to iterate for a maximum of five steps.

3.2. Vessel selection

Commencing with the initial over-segmentation, each iteration step attempts to remove false positives while keeping true positives. Since practically the removal of all falsely detected segments as well as the preservation of true vessel segments is not guaranteed, the user may choose the desired vessel segments from each intermediary segmentation result by specifying (by mouse click) a point on the vessel. This point is then used as seed and all segmented vessel points connected to it (by an eight points neighborhood) are selected in the final segmentation. Results are shown in Fig. 1f and Fig. 2c.

4. RESULTS AND EXPERIMENTS

As of present we have used 11 micro-angiograms from our data base to evaluate our algorithm both with respect to the quality of the feature extraction process and the segmentation results. Before processing, to increase the computations' speed, and because generally, the size of the smallest interesting vessel is larger than the minimal attainable resolution, the analyzed images were downsampled from the original 512x512 pixels to 256x256. As reference we have used manual segmentation results performed by the first author. The outcome of the vessel filtering procedure should be a separable feature space. The separability is measured by the J_1 criterion [7, p. 446]. Table 1 shows the results obtained for each vessel map (feat1-3), for the entire pixel feature vector space (3D-feat_sp) and for the original micro-angiogram (org). Clearly, the pixel feature space yields good results. The size of the morphological filter window was 13 pixels. For the homomorphic filter we have used a multiplication factor of two and a Gaussian low-pass kernel of size seven with a standard deviation of 1.5. The eigenvalues of the Hessian matrix were calculated at four scales. The segmentation performance is evaluated by the mean percentages of correct classifications (CC) and false positives (FP). In Table 2 we present the results obtained

Table 1. Separability measured by the $J1$ criterion.

	feat1	feat2	feat.3	3D-feat_sp	org
J1	0.6510	0.2012	0.5737	0.8025	0.1506

Table 2. Segmentation results.

CC-user	FP-user	CC-no_user	FP-no_user
81.0345	3.6682	60.3175	2.5061

by the semi-automatic algorithm (-user) as well as the results obtained without user intervention (-no_user). In the latter case, we have used an additional separability based stopping criterion [4] and the algorithm iterated for four to six steps. Results are shown in Fig. 1e and f respectively and in Fig. 2. Most of the false positives, for the semi-automatic algorithm, appear in the vicinity of vessels. At a repeated visual inspection some of these were reclassified as real vessels not captured in the initial "ground truth". Thus the values of Table 2 should be regarded as the lower and upper bounds for the percentages of correct classifications and that of false positives, respectively.

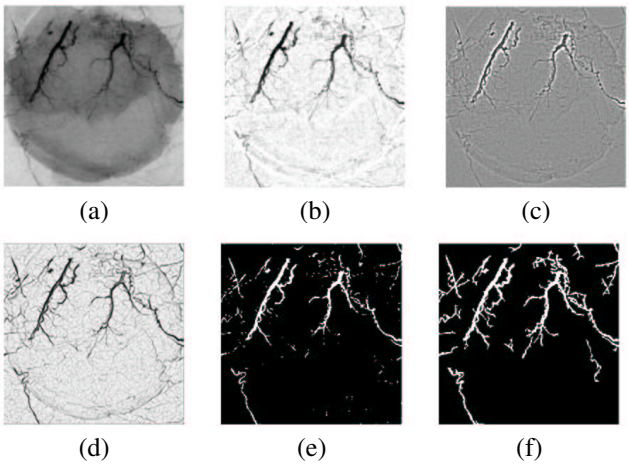

(a) (b) (c)

(d) (e) (f)

Fig. 1. Original micro-angiogram (a), result of morphological processing (b), homomorphic filtration (c), analysis of the eigenvalues of the Hessian matrix (d), automatic segmentation (e) and segmentation, after selection by user supplied seed points (f).

5. CONCLUSIONS AND DISCUSSION

We have presented a novel framework for imaging and analysis of micro-vessels in skin transplants in laboratory environments for drug testing. For imaging, a specific micro-angiography technique was described, followed by an analysis algorithm which provides automatically a reasonable, though in general not error-free, result. This result may then be edited comfortably and quickly by the experimenter by stepping through a low number of intermediate results. Central to the analysis part is a micro-vessel segmentation algorithm, the results of which will be used for vessel area and vessel length measurements in skin transplant micro-angiograms. Our system is now in routine use, results obtained from larger numbers of transplant samples will be reported in the near future.

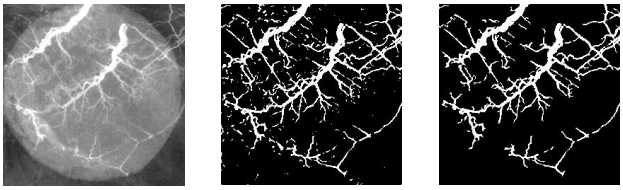

(a) (b) (c)

Fig. 2. Original micro-angiogram (a), automatic segmentation (b) and user supported segmentation (c).

6. REFERENCES

[1] T. Aach, C. Mayntz et al., "Spatiotemporal multiscale vessel enhancement for coronary angiograms," *MI02*, SPIE-4684:1010–1021, 2002.

[2] E. Backer and A.K. Jain, "A clustering performance measure based on fuzzy set decomposition," *IEEE T PAMI*, 3(1):66–75, 1981.

[3] Z. Chen and S. Molloi, "Multiresolution vessel tracking in angiographic images using valley courses," *Opt. Eng.*, 42:1673–1682, 2003.

[4] A. Condurache, T. Aach et al., "Vessel segmentation and analysis in laboratory skin transplant micro-angiograms," *Proc. of CBMS*, to appear, 2005.

[5] E.R. Dougherty, "Mathematical morphology in image processing," *Marcel Dekker*, 1992.

[6] A. F. Frangi, W. J. Niessen et al., "Multiscale vessel enhancement filtering," *MICCAI*, LNCS 1496:130–137, 1998.

[7] K. Fukunaga, "Introduction to statistical pattern recognition," *Academic Press*, 1990.

[8] S. Grzybowski, B. Bucsky et al., "Model for induction of angiogenesis by synergetic effects of BFGF and VEGF^{165} by bioactive dermal matrices," *LAS*, 389(10), 2004.

[9] S. Grzybowski, B. Bucsky et al., "A microangiography technique to quantify fasciocutaneous blood vessels in small laboratory animals," *LAS*, 389(10), 2004.

[10] X. Jiang and D. Mojon, "Adaptive local thresholding by verification-based multithreshold probing with application to vessel detection in retinal images," *IEEE T PAMI*, 25(1):131–137, 2003.

[11] C. Kerbas and F.K.H. Quek, "A review of vessel extraction techniques and algorithms," http://vislab.cs.vt.edu/review /extraction.html, 2002.

[12] A.V. Oppenheim R.W. Schafer et al., "Nonlinear filtering of multiplied and convolved signals," *Proc. of IEEE*, 56(8):1264–1291, 1968.

[13] R Poli and G Valli, "An algorithm for real time vessel enhancement and detection," *Comp. Meth. and Prog. in Biomed.*, 52(1):1–22, 1997.

[14] D. Selle, B. Preim et al., "Analysis of vasculature for liver surgical planning," *IEEE T MI*, 21(11):1344–1357, 2002.

[15] R. Toledo, X. Orriols et al., "Eigensnakes for vessel segmentation in angiography," *Proc. of ICPR*, 2002.